A Polarization and Radiation Beam Reconfigurable Integrated Antenna With Broadband and High Gain for mmWave Vehicular Communication

Yaling Chen, *Member, IEEE*, Long Zhang, *Member, IEEE*, Yejun He, *Senior Member, IEEE*, and Zhi Ning Chen, *Fellow, IEEE*

***Abstract*—A novel integrated antenna supporting polarization and radiation beam reconfigurability is proposed for emerging millimeter-wave (mmWave) vehicular communication. To meet the reconfigurability requirement of the vehicular communication system, a compact shared-aperture two-dimensional leaky-wave antenna (LWA) is designed. The LWA is generated by the parallel-plate waveguide (PPW) long-slot structure and its open stopband issue is suppressed completely by employing a unit cell with two asymmetrical slots, leading to high-gain and broadband characteristics. Besides, a multifunction feeding network constituted by four switchable input ports, four parabolic reflector systems, and an integrated multifunction coupler is seamlessly incorporated with the radiation aperture within a single substrate, realizing a low-cost solution for vehicular communication applications. Based on the proposed design concept, a broadband high-gain integrated antenna featuring polarization and radiation beam reconfigurability is engineered, fabricated, and installed into an antenna measurement system for validation. Experimental results demonstrate that the proposed antenna achieves a peak gain of 23.6 dBi together with a bandwidth of 56.6% from 19 GHz to 34 GHz. Additionally, it exhibits good polarization and radiation beam reconfigurable capability, providing horizontal/vertical linear-polarization single-beam, right-/left-handed circular-polarization single-beam, and dual-linear-polarization equal/unequal-amplitude dual-beam operating capability. Furthermore, a wide beam scanning coverage of 105° in *xoz*-plane and 108° in *yoz*-plane is achieved by the presented design. The extraordinary advantages of the proposed integrated antenna such as wide bandwidth, high gain, polarization and radiation beam reconfigurability, and low cost make it suitable for various millimeter-wave vehicular communication application scenarios.**

***Index Terms*—Two-dimentional leaky-wave antenna (LWA), integrated antenna, millimeter-wave vehicular communication, polarization reconfigurability, radiation beam reconfigurability.**

Received 7 July 2024; revised 12 October 2024 and 6 November 2024; accepted 10 November 2024. Date of publication 13 November 2024; date of current version 5 March 2025. This work was supported in part by the National Key Research and Development Program of China under Grant 2023YFE0107900, in part by the National Natural Science Foundation of China under Grant 61801299 and Grant 62071306, in part by the Natural Science Foundation of Guangdong Province under Grant 2020A1515011037, and in part by Shenzhen Science and Technology Program under Grant JSGG20210420091805014, Grant JSGG20210802154203011, and Grant JCYJ20230808105510020. The review of this article was coordinated by Dr. Subhradeep Chakraborty. *(Corresponding author: Yejun He.)*

Yaling Chen, Long Zhang, and Yejun He are with the State Key Laboratory of Radio Frequency Heterogeneous Integration, Shenzhen 518060, China, also with the Sino-British Antennas and Propagation Joint Laboratory of Ministry of Science and Technology of China, Shenzhen 518060, China, also with the Guangdong Engineering Research Center of Base Station Antennas and Propagation, Shenzhen 518060, China, and also with the Shenzhen Key Laboratory of Antennas and Propagation, College of Electronics and Information Engineering, Shenzhen University, Shenzhen 518060, China (e-mail: chenyaling4068@163.com; long.zhang@szu.edu.cn; heyejun@126.com).

Zhi Ning Chen is with the Department of Electrical and Computer Engineering, National University of Singapore, Singapore 119077 (e-mail: eleczn@nus.edu.sg).

Digital Object Identifier 10.1109/TVT.2024.3497657

I. Introduction

VEHICULAR communication is one of the key technologies for supporting the Internet of Vehicles (IoV) [1]. Vehicular communication is essential for enhancing road safety, improving traffic efficiency, and enabling autonomous driving. Given the rapid advancements in modern intelligent IoV, a vehicle-to-everything (V2X) communication system should be built to meet the requirement of various practical IoV application scenarios, including the vehicle-to-vehicle (V2V), vehicle-to-infrastructure (V2I), vehicle-to-network (V2N), and vehicle-to-pedestrian (V2P) [2], [3]. Reconfigurable antennas are indispensable in vehicular communication systems [4], [5]. In particular, antennas operating at mmWave frequency bands hold considerable promise for diverse application scenarios of vehicular communication, including modern intelligent vehicular networks, high-speed intelligent transportation systems, etc [6]. However, owing to the shorter wavelength of electromagnetic (EM) waves at mmWave frequency bands, the absorption of atmosphere and water molecules tends to induce high path losses, thereby reducing communication range [7]. This means that a high-performance antenna is highly desired for mmWave vehicular communication [8], [9], [10], [11]. As one of the critical radio-frequency modules, antennas act as the "eyes" for transmitting or receiving signals in various wireless communication systems. A three-element circularly polarized multiple-input-multiple-output (CP-MIMO) antenna system with spatial diversity, pattern diversity, and polarization diversity was proposed for V2X communications [12]. To meet the strict requirements of mmWave vehicular communication systems, the need for reconfigurable antennas, such as polarization reconfigurability and radiation beam reconfigurability is rapidly increasing [4], [5]. Accordingly, as shown in Fig. 1, the reconfigurable antenna should be designed to meet the V2X communication requirement of IoV applications, such as V2V and V2I communications. As shown, reconfigurable antenna

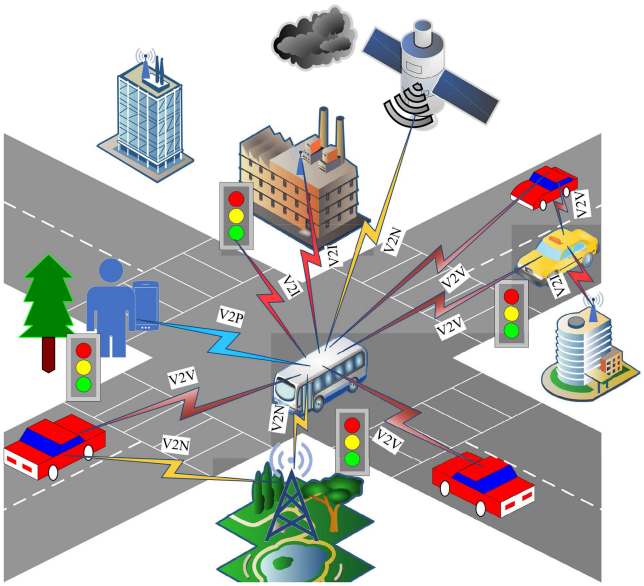

Fig. 1. An illustration of the utilization of the reconfigurable antenna in different vehicular communication application scenarios.

supporting polarization and radiation beam reconfigurability needs to be developed. Moreover, low-cost antenna is also necessary for practical vehicular communication applications.

Accordingly, the wireless requirements of IoV facilitates the innovation of low-cost reconfigurable antennas that can generate polarization reconfigurability while maintaining radiation beam reconfigurability. To satisfy the requirement of the reconfigurable antenna, leaky-wave antenna (LWA) is used and investigated in this study. LWAs are a kind of promising alternative for mmWave vehicular applications because of their high directivity, broad bandwidth, frequency-controlled beam-scanning capability, low cost, simple feeding networks [13], [14]. LWAs are a common type of traveling-wave antennas, characterized by the propagation of EM waves in one direction and gradual leakage along guiding-wave structure [15], [16], [17], [18]. Parallel-plate waveguide (PPW)-based LWA is an effective, scalable alternative to improve the antenna gain [19], [20], [21], [22], [23], [24]. However, these antennas were generally designed as single-polarization single-beam antennas. Although dual-polarized PPW LWAs were presented by switching the transmission path of the input signal [22], [23], [24], the employed multi-layer structure undoubtedly increased the antenna complexity and the cost of fabrication. Typically, they had a fixed broadside beam and were intended to be directional antennas. Moreover, only two polarization states can be chosen.

Polarization reconfigurable LWAs can dynamically change their polarization states according to the needs of practical IoV applications. This feature provides great flexibility and polarization diversity for vehicular communication systems, effectively mitigating multipath fading and enhancing channel capacity [25], [26], [27], [28], [29]. An LWA based on half-mode SIW was introduced in [26], capable of dynamically processing quad-polarization states depending on the specific input ports of excitation. Nonetheless, only one beam could scan within one quadrant with $<30^\circ$ coverage in each polarization state. Recently, an LWA featuring polarization diversity was presented, and four beams could be generated to scan simultaneously [28]. However, the polarization reconfigurability of this antenna was realized by varying different extended dividers, increasing the complexity of measurement [28]. Although an SSPP-based LWA without a complex feeding network was designed to realize multibeam and multi-polarized radiation, the bandwidth and antenna gain were limited by its operating mode and small radiation aperture, respectively [29]. In [30], a radiation-beam reconfigurable PPW-based LWA was designed by using a pillbox transition and seven input ports. However, it can only realize one single polarization [30]. Although dual-polarized antennas could be achieved by switching the input ports [22], [23], [24], only a fixed beam at the broadside was obtained, reducing the beam-scanning coverage. Therefore, designing a wide beam-scanning LWA with polarization and radiation beam reconfigurability is still a tough challenge.

A broadband high-gain LWA-based antenna with polarization and radiation beam reconfigurability is proposed for mmWave vehicular communication in this paper. The feeding network consists of four switchable input ports, four parabolic reflector systems, and a multifunction coupler. By switching the input ports, different polarization states, encompassing horizontal and vertical linear polarization (LP) states, as well as right-handed and left-handed circular polarization (RHCP & LHCP) states, can be obtained. Moreover, a dual-polarization dual-beam radiation can be realized by using the proposed multifunction coupler and varying the operating frequency. Specifically, when Port 3 or 4 is excited and the beam scans to the broadside direction, a CP radiation is generated. Then, the dual-polarization dual-beam radiation is achieved in two orthogonal planes while the antenna operates in the backward or forward scanning frequency region. It is noted that the amplitude difference of the two beams can be reconfigured by adjusting the power difference between two output ports of the multifunction coupler. Moreover, when the multifunction coupler is operating as a crossover, a single-polarization single-beam radiation is implemented.

II. Antenna Design and Analysis

Fig. 2 shows the top view of the proposed reconfigurable PPW LWA. As shown, the proposed LWA comprises a feeding network and a radiation aperture. The proposed feeding network contains four input ports, four grounded coplanar waveguide (GCPW)-SIW transitions, four small SIW H-plane horns, four offset parabolic reflectors, and a multifunction coupler. The GCPW-SIW transition provides wideband impedance matching from the GCPW to the SIW (19–34 GHz). The radiation aperture is engraved on the upper layer of a substrate. The whole antenna is built on a Rogers RO4003C substrate, which has a loss tangent of 0.0027 and a dielectric constant of 3.55, measuring 1.524 mm thick. The copper foil has a thickness of 0.018mm. The total dimension of the proposed antenna is $177.4 \times 177.4 \times 1.56\ \text{mm}^3$ and its radiation aperture size is $87.1 \times 87.1\ \text{mm}^2$.

The 2-D radiation aperture is centered within the substrate. Each antenna unit cell contains two asymmetric long-straight slots to eliminate the open stopband (OSB) completely. The

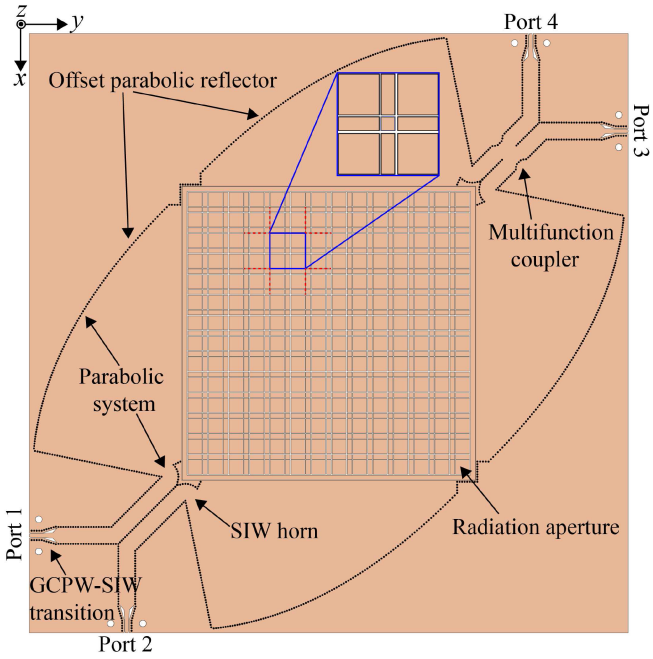

Fig. 2. Geometry of the proposed reconfigurable PPW LWA.

2-D LWA is generated by four rotational symmetrical 1-D LWA subarrays. Four offset parabolic reflectors are designed to excite the radiation aperture. Such an offset parabolic reflector can reduce the feeding complexity and the via number of the feeding network compared to the traditional 2^N-way SIW power dividers. As depicted in Fig. 2, upon excitation of Port 1, the EM wave enters the left reflector where it is transformed into a plane wave, subsequently advancing into the radiation aperture along the y-axis. In such way, a y-directed horizontal LP radiation with high gain is implemented. Similarly, an x-directed vertical LP radiation can be realized by the excitation of Port 2. By exciting Port 3 or 4, one pair of orthogonal equal-amplitude plane waves with 90° phase difference can be generated for the proposed LWA due to the addition of multifunction coupler. A RHCP or LHCP radiation at broadside direction can be obtained by exciting Port 3 or 4, respectively. When the antenna operates in the backward- or forward-direction region, a dual-polarization dual-beam radiation is achieved in two orthogonal planes. It is noted that the amplitude difference of the two beams can be dynamically changed by adjusting the power difference between two output ports of the multifunction coupler. Moreover, a single-polarization single-beam radiation is implemented when the proposed coupler operates as a crossover.

A. Analysis of the PPW LWA Unit Cell

Fig. 3 displays the unit cell with periodic boundary. The two nonidentical slots in the proposed unit cell are utilized to fully suppress the OSB [31], [32]. The caption of Fig. 3 contains a list of the optimal dimensions of the proposed unit cell. Based on the proposed unit cell, the dispersion diagram can be extracted by following equations [33]:

$$\beta_{eff} = \frac{1}{p}\,\mathrm{Im}\left[\cosh^{-1}\left(\frac{1 - S_{11}S_{22} + S_{12}S_{21}}{2S_{21}}\right)\right] \quad (1)$$

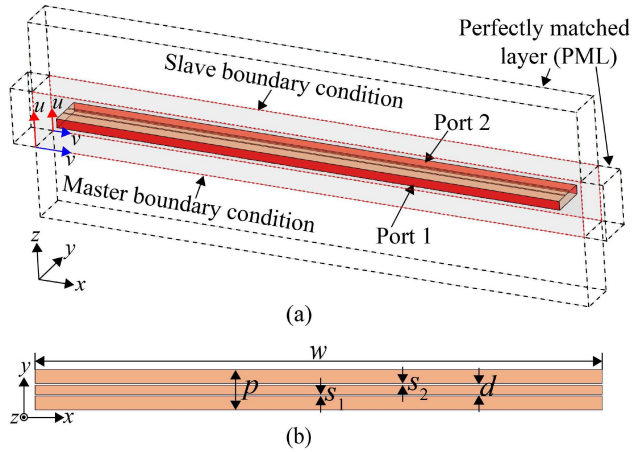

Fig. 3. (a) Simulation model of the single unit cell. (b) Top view of the proposed asymmetrical unit cell ($p = 6.1$ mm, $d = 1.66$ mm, $s_1 = 0.2$ mm, $s_2 = 0.3$ mm, $w = 87$ mm).

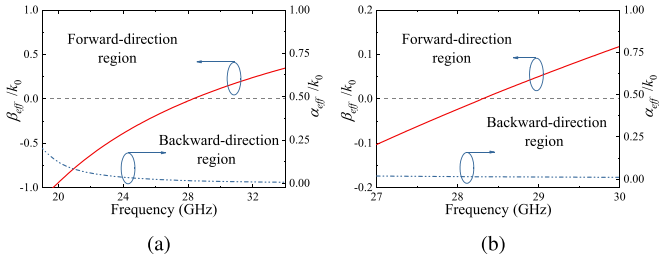

Fig. 4. (a) Normalized phase and attenuation constant of the unit cell. (b) Magnified figure of (a).

$$\alpha_{eff} = \frac{1}{p}\,\mathrm{Re}\left[\cosh^{-1}\left(\frac{1 - S_{11}S_{22} + S_{12}S_{21}}{2S_{21}}\right)\right] \quad (2)$$

where the unit cell is treated as a two-port network to acquire the S-parameters, as shown in Fig. 3. The values of β_{eff}/k_0 and α_{eff}/k_0 are determined by computing (1) and (2), as illustrated in Fig. 4. As indicated by Fig. 4, the OSB problem is eliminated completely.

B. Analysis of the Proposed LWA

Actually, the proposed unit cell has two asymmetrical slots, leading to a conventional asymmetrical 1-D antenna array. However, in this case, the reflection coefficients of two ports for the asymmetrical antenna array are different. To realize a symmetrical antenna array, two sub-arrays (Sub-array #1 and #2) are arranged symmetrically by the middle line of the array to achieve the proposed 1-D periodic LP LWA, as illustrated in Fig. 5(a). Cell A is defined as the unit cell with a smaller slot etched on the left-hand side and a wider slot placed on its right side. Cell B is the opposite one. A cell with two symmetrical slots (Cell C) is placed in the middle of the 1-D LWA to provide a connection between the Sub-array #1 and #2, as shown in Fig. 5(b). It can be seen from Fig. 5 that Sub-array #1 is designed based on Cell A, while Sub-array #2 is implemented by Cell B. This arrangement ensures that the proposed 1-D LWA is configured symmetrically. The simulated reflection coefficients of each part of the 1-D LWA are shown in Fig. 6. As shown,

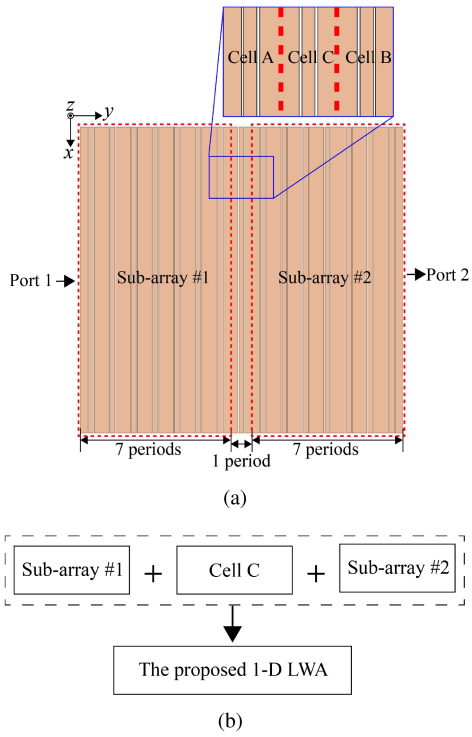

Fig. 5. (a) Illustration of the proposed 1-D periodic LWA. (b) Evolution of the proposed 1-D LWA.

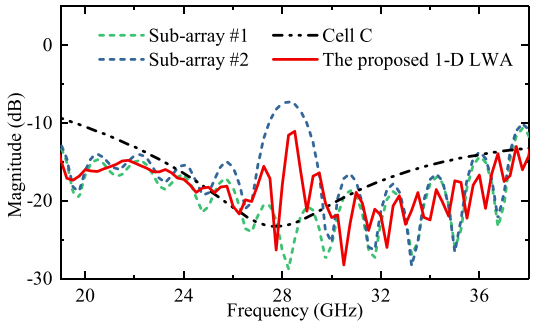

Fig. 6. Simulated reflection coefficients of each part of the 1-D periodic LWA.

Sub-array #1 and Cell C have a wide operating frequency band of 19–38 GHz. It can be seen from Fig. 6 that the reflection coefficient of Sub-array #2 is different from that of Sub-array #1. The reason for this phenomenon is the different alignment of the slots. Although the reflection coefficient of Sub-array #2 is greater than −10 dB around 28.25 GHz, the $|S_{11}|$ of the final design is less than −10 dB within the whole frequency band of 19–38 GHz due to the existence of Sub-array #1 and Cell C. Therefore, Sub-array #1 and Cell C are not only radiators but also the impedance transformers of Sub-array #2. Since the proposed 1-D LWA is symmetrical, the reflection coefficients from both sides of the 1-D LWA are the same, which are not shown here for brevity.

Utilizing the proposed 1-D LWA, a 2-D LWA is implemented by placing the two same 1-D LWA orthogonally, as depicted in Fig. 2. Such a radiation aperture is designed to achieve

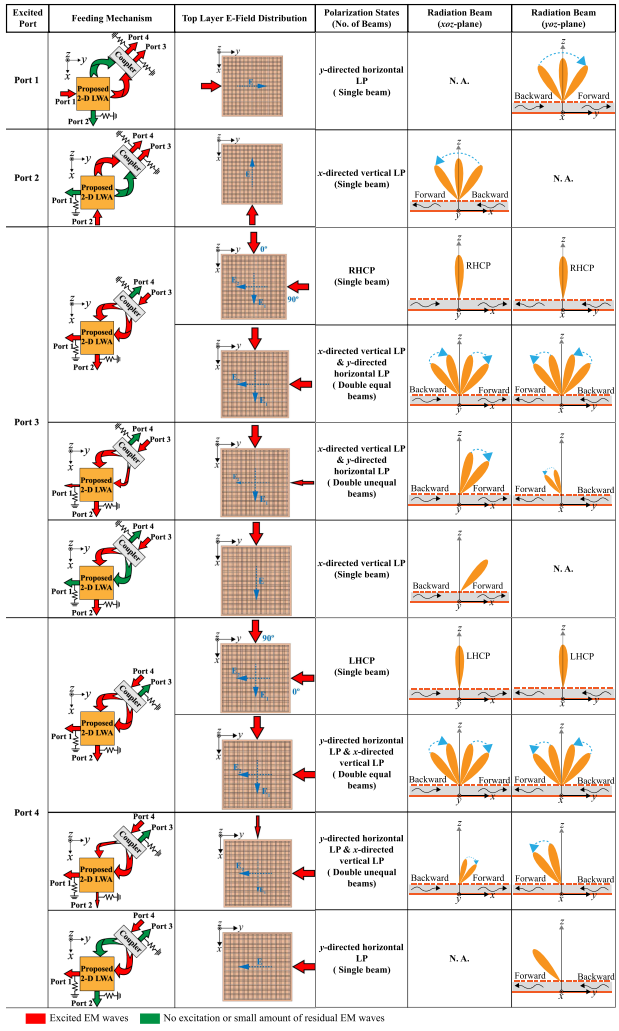

Fig. 7. Operating principle of the proposed LWA.

polarization and radiation beam reconfigurability, which would be described in detail in Section II-C.

C. Polarization and Radiation Beam Reconfigurability

As shown in Fig. 2, four switchable input ports and a multifunction coupler are used to obtain the polarization and radiation beam reconfigurability. The operating principle of the proposed LWA is detailed in Fig. 7. Based on the means of excitation and electric field orientation, the polarization states and radiation beam are systematically investigated. Regarding the feeding mechanism in Fig. 7, the red arrows represent the excited EM waves, while the green arrows represent no excitation or a small amount of residual EM waves. The dispersion characteristic of the proposed PPW unit cell indicates that the antenna scans in the backward quadrant over the frequency band of 19–28.3 GHz, and in the forward quadrant within the frequency range of 28.3–34 GHz. Broadside beam occurs at the frequency of 28.3 GHz, which has been given in Fig. 4. Besides, it is noted in Fig. 7 that the proposed multifunction

coupler has three kinds of operating states, e.g., equal-amplitude coupler, unequal-amplitude coupler, and crossover states. When the amplitude difference between the two output ports of the coupler is lower than 3 dB, the coupler is defined as an equal-amplitude power divider, otherwise it is an unequal-amplitude power divider. Moreover, when the amplitude difference exceeds 10 dB, the coupler is defined as a crossover. Therefore, Fig. 7 shows that the polarization reconfigurability and radiation beam reconfigurability are simultaneously controlled by the switching of the input ports, the change of the operating frequency and the energy distribution of the coupler.

The basic principle of the proposed antenna is explained as follows. When Port 1 is excited, while keeping other ports terminated with a matched load, the incident EM wave is converted into a plane wave by the reflector system, which is radiated outside along the *y*-direction of the radiation aperture and absorbed at Ports 3 and 4. In this case, a *y*-directed horizontal LP radiation with single-beam operation is implemented and its radiation beam scans from the backward to forward direction within the *yoz*-plane. Similarly, an *x*-directed vertical LP is achieved when the excitation is switched to Port 2. In this case, the antenna scans in *xoz*-plane. Thus, a single-polarization single-beam is obtained by exciting Port 1 or 2. When Port 3 is excited, there are four operating states by simultaneously controlling the operating frequency and the energy distribution of the coupler, as depicted in Fig. 7. The first operating state is the CP radiation state. When Port 3 is excited, the incident wave is split into two equal-amplitude components with a 90° phase shift. These two parts of EM waves are transmitted to two orthogonal sides of the proposed 2-D LWA, forming two orthogonal plane waves to excite the two adjacent sides of the radiation aperture. In this case, two beams are generated in two orthogonal planes (*xoz*- and *yoz*-plane). When these two beam all scans to the broadside direction, a RHCP radiation can be obtained [22]. The second state is an equal-amplitude dual-polarization dual-beam radiation state which is achieved when the antenna operates at the backward or forward frequency region and the proposed coupler provides a pair of equal-amplitude outputs. Furthermore, the third state is the dynamic amplitude dual beams when the coupler provides a pair of unequal-amplitude outputs. The amplitude difference between two beams can be dynamically controlled by directly changing the power difference between two output ports of the proposed coupler. The final state is an *x*-directed vertical LP beam if the coupler is changed to a crossover. Similarly, when Port 4 is excited, four operating states are changed correspondingly, including LHCP, equal/unequal-amplitude dual-polarization dual-beam, and *y*-directed horizontal LP radiation.

For clearer demonstration, the 3-D radiation patterns of the proposed LWA when excited by Ports 1 and 3 at four operating frequencies are illustrated in Figs. 8 and 9, respectively. As shown in Fig. 8, a *y*-directed horizontal LP radiation is realized and the radiation beam scans from backward to forward within the *yoz*-plane. As for Fig. 9, RHCP, equal/unequal-amplitude dual-polarization dual-beam, and *x*-directed vertical LP radiations are achieved when Port 3 is excited. Therefore, the polarization and radiation beam reconfigurability can be achieved by the proposed antenna.

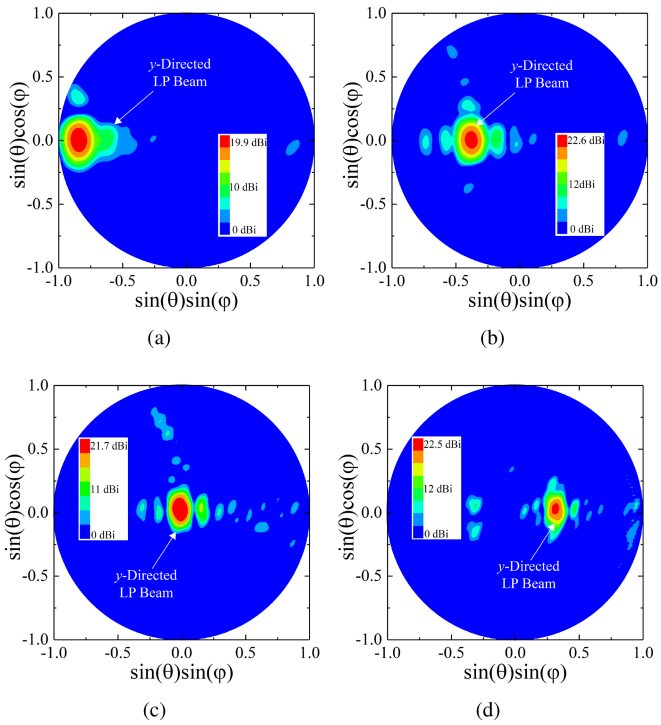

Fig. 8. Simulated 3-D radiation patterns of the proposed LWA excited by Port 1 at four different frequencies. (a) 20 GHz, (b) 24 GHz, (c) 28.25 GHz, and (d) 33.5 GHz.

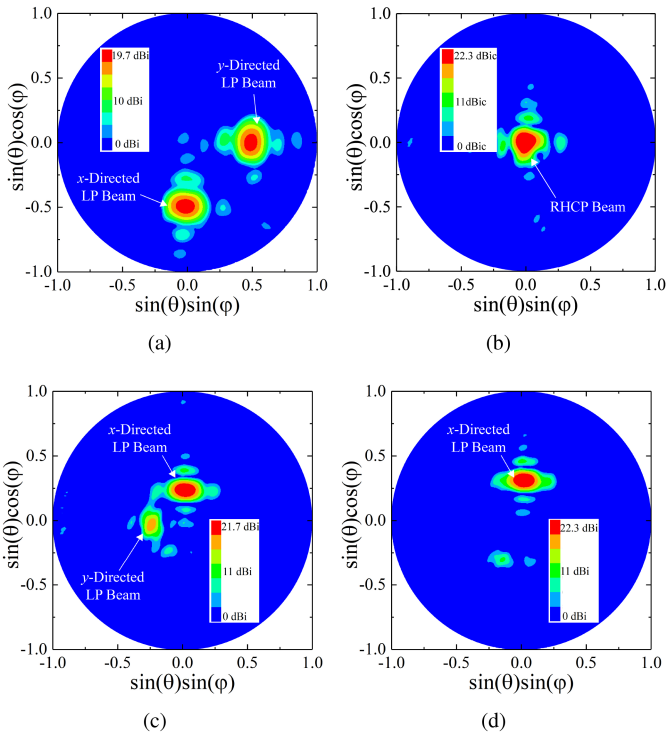

Fig. 9. Simulated 3-D radiation patterns of the proposed LWA excited by Port 3 at four different states. (a) Equal-amplitude dual-polarization dual-beam radiation, (b) RHCP radiation, (c) Unequal-amplitude dual-polarization dual-beam radiation, and (d) *x*-directed vertical LP radiation.

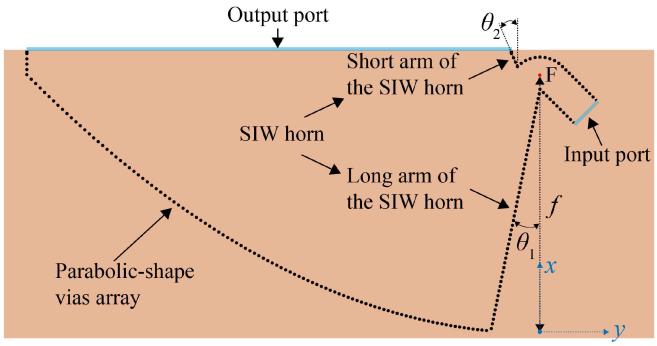

Fig. 10. Geometry of the offset parabolic reflector system (θ_1 =11.5°, θ_2 =25°, f = 40 mm).

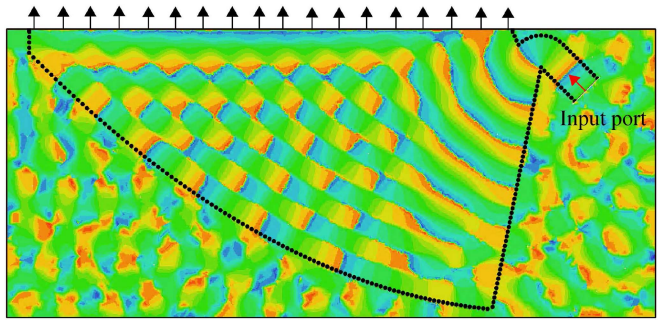

Fig. 11. Phase distribution of the electric field of the proposed offset parabolic reflector system.

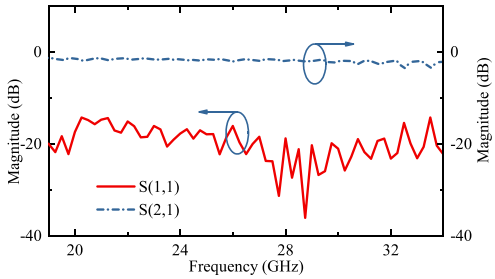

Fig. 12. Simulated S-parameters of the offset parabolic reflector system. (Input port is defined as Port 1, while the output port is Port 2).

III. Design of the Integrated Feeding Network

In this design, a feeding network for the proposed antenna is integrated with the radiation aperture within a single substrate, by employing four GCPW-SIW transitions, four offset parabolic reflector systems and a multifunction coupler. Four GCPWs is used as the antenna feed, and a GCPW-to-SIW transition is placed between the GCPW and the SIW for transforming quasi-TEM mode to TE_{10} mode. The tapered width of the GCPW-to-SIW transition is selected to ensure smooth transition of the characteristic impedance from the GCPW to SIW. With the aid of HFSS, excellent performances of the feeding structure are obtained. The reflection coefficient and the insertion loss of this feeding structure are smaller than −20 dB and 0.75 dB over the whole operating band, respectively.

A. Design of the Offset Parabolic Reflector System

To achieve an antenna with high-gain performance, a uniform wavefront is required for illuminating the proposed PPW LWA. In this design, the offset parabolic feeding system is utilized to provide a plane-wave illumination for PPW LWA. Such offset feeding mechanism generates no blockage to the reflected waves so that the feeding network can be integrated into the same substrate of the radiation aperture. The geometry of the parabolic reflector system is displayed in Fig. 10. As shown, the system contains a parabolic-shaped array of vias and a SIW horn. The configuration of the parabolic reflecting vias array can be defined by

$$y^2 = 4fx \tag{3}$$

where f is the focal length. The optimal parameters of this reflector system are given in Fig. 10. Besides, the long arm of the SIW horn is tilted by 11.5° to guide EM waves to the middle of the reflector. Both arms of the horn are designed to suppress the propagation of EM waves outside the reflector boundary and confine the EM waves inside the system.

The operating principle of the proposed parabolic system is described as follows. The phase distribution of the electric field within the feeding system is shown in Fig. 11. As demonstrated, when the phase center of the horn is positioned at the focal point F of the reflector, the incident waves from the SIW horn illuminate the offset parabolic reflector and are changed to plane waves travelling in the direction perpendicular to the aperture of parabola. Therefore, a uniform quasi-TEM wavefront is created at the aperture of the parabolic system, thereby yielding high gain. As depicted in Fig. 12, the simulated reflection coefficient $|S_{11}|$ of the input port is below −14.2 dB, and the average insertion loss from the input port to the output port is around 1.8 dB.

B. Design of the Multifunction Coupler

The multifunction coupler is a crucial component in this work, which controls the polarization and radiation beam states of the proposed antenna. In this design, three kinds of operating states, e.g., equal-amplitude coupler, unequal-amplitude coupler, and crossover, are needed for the design of the proposed multifunction coupler. Note that conventional couplers generally work in a single operating state, such as the equal-amplitude coupler, resulting in a limited operating frequency band and a single coupler function. However, the coupler designed in this work realizes three working states by expanding its operating bandwidth. Fig. 13 illustrates the configuration of the proposed coupler and its optimized dimensions. Its S-parameters are shown in Fig. 14(a). It can be observed that the reflection coefficients of Port 1 are less than −10 dB from 22 GHz to 34 GHz. Besides, isolation between two adjacent ports (Ports 1 and 2) is higher than 10 dB within the operating frequency range. The phase imbalances between two output ports (Ports 3 and 4) are also given in Fig. 14(b). As shown, the phase imbalances are around 90° in the frequency band of 23–32 GHz. Fig. 15 shows the magnitude imbalances of two output ports. It can be seen that there are three operating states, e.g., equal-amplitude, unequal-amplitude coupler, and crossover. It is noted that the coupler is defined

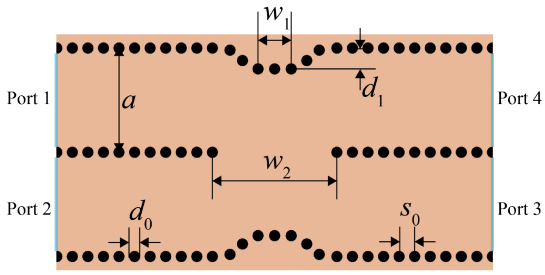

Fig. 13. Top view of the proposed coupler. ($a = 5$ mm, $d_0 = 0.5$ mm, $d_1 = 1$ mm, $s_0 = 0.75$ mm, $w_1 = 1.6$ mm, $w_2 = 6$ mm).

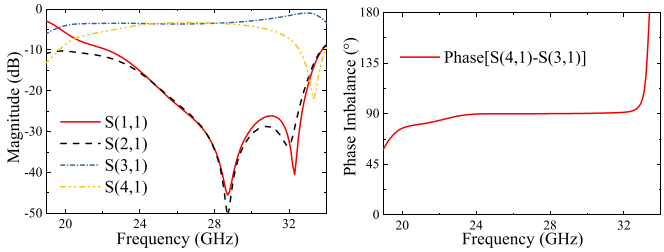

Fig. 14. (a) Simulated S-parameters and (b) Phase imbalance of the proposed coupler.

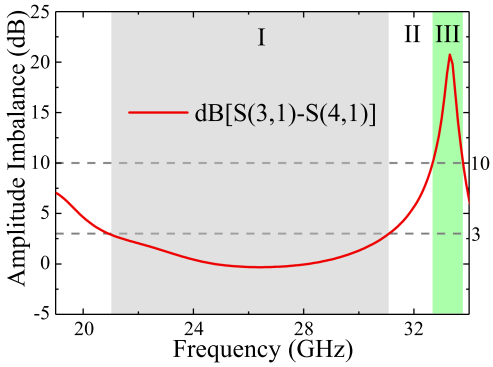

Fig. 15. Simulated amplitude imbalance of the proposed coupler (Region I: equal-amplitude coupler, Region II: unequal-amplitude coupler, and Region III: crossover.).

as an equal-amplitude coupler when the amplitude difference is lower than 3 dB, otherwise it is an unequal-amplitude coupler. Moreover, if the amplitude difference exceeds 10 dB, the coupler is defined as a crossover. Therefore, three operating states are achieved when frequency varies.

IV. Results and Discussions

To experimentally validate the design concept and methodology, the proposed antenna is constructed on a single substrate by low-cost PCB fabrication technology. As shown in Fig. 16, four standard 2.92-mm connectors are assembled to the antenna so that the antenna can be connected to the measuring facilities.

The simulated and measured S-parameters of Port 1 and Port 3 are shown in Figs. 17 and 18, respectively. The measured S-parameters are obtained by Keysight network analyzer. As shown, the measured curves show a good matching with the

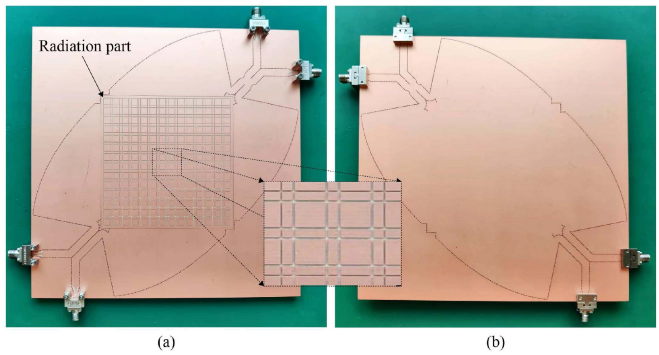

Fig. 16. Fabricated prototypes. (a) Top view. (b) Bottom view.

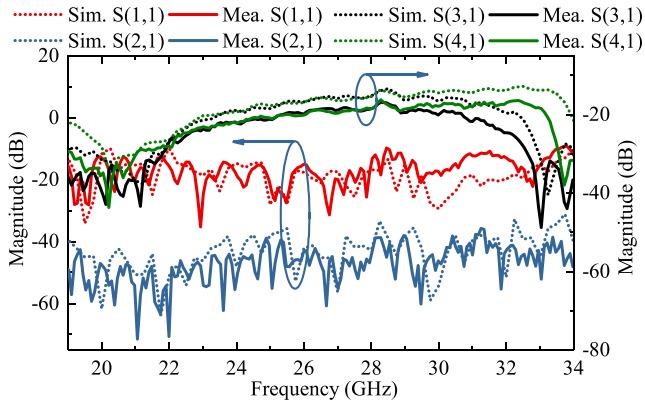

Fig. 17. Comparison of simulated and measured S-parameters for the proposed LWA excited by Port 1.

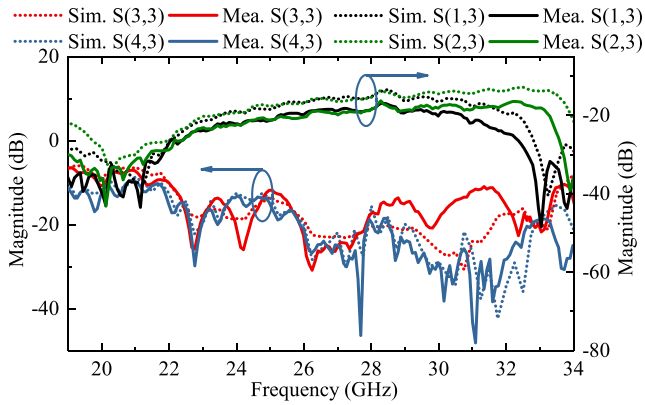

Fig. 18. Comparison of simulated and measured S-parameters for the proposed LWA excited by Port 3.

simulated ones. As depicted in Figs. 17 and 18, the reflection coefficients of Port 1 are all below −10 dB within 19–34 GHz, and the reflection coefficients of Port 3 are all below −10 dB within 22–34 GHz. The bandwidth difference between Port 1 and Port 3 is the addition of a coupler with a limited operating frequency of 22–34 GHz. Besides, all the isolations are all better than 10 dB within the operating band. Especially, a high isolation around 35 dB is obtained between Port 1 and Port 2. Besides, the transmission coefficients (such as $|S_{31}|$ and $|S_{41}|$) are also below −10 dB, which means that most of EM waves are radiated out. The results for Port 2 and Port 4 are not illustrated here, as they are similar to those for Ports 1 and 3, respectively.

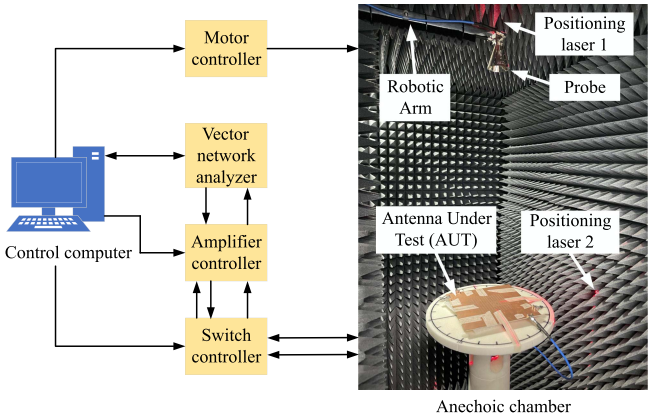

Fig. 19. Near-field antenna measurement system for the proposed antenna in the anechoic chamber.

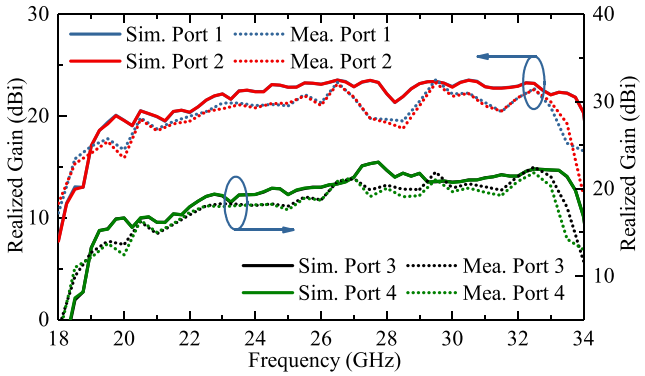

Fig. 20. Simulated and measured gains of the proposed antenna excited by different input ports.

For the measured radiation performance of the proposed antenna, the near-field antenna measurement system by an anechoic chamber is used, as illustrated in Fig. 19. As shown, a computer is used to control the anechoic chamber and analyze the measured results. During measurement, only one port is connected to the transmission line, while the other three ports are connected to a matching load, respectively. In this way, the antenna radiation performance of one excited port can be tested. Then, the excited port is switched so that the radiation performance of all four ports can be tested one by one.

Fig. 20 shows the gain performances of four ports. It can be seen that the measured gains are slightly lower than the simulated results because of the measured errors and the loss of connectors. The simulated gains of two adjacent ports (Ports 1 and 2, Ports 3 and 4) are almost the same. The maximum measured gains of Ports 1 and 2 are 23.6 dBi at 29.5 GHz and 23.3 dBi at 29.5 GHz, respectively. For Ports 3 and 4, the peak gains are 22.5 dBi at 32.5 GHz and 21.8 dBi at 32.5 GHz, respectively. For all ports, the measured gains are higher than 15 dBi over the operating frequency band. It is noted that the measured gains are shifted to the lower frequency by about 0.25 GHz compared to the simulated ones, which may be attributed to the dielectric constant difference and fabrication errors of the LWA during the manufacturing.

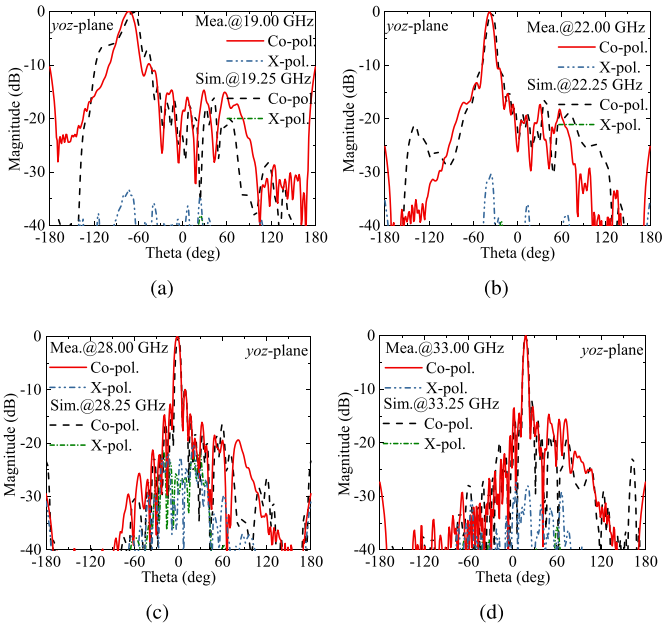

Fig. 21. Measured and simulated radiation patterns of the proposed antenna excited by Port 1 at four different frequencies. (a) 19 GHz. (b) 22 GHz. (c) 28 GHz. (d) 33 GHz.

Fig. 21 illustrates the *y*-directed horizontal LP radiation patterns in the *yoz*-plane for Port 1. As shown, the simulated beam scans from −67° to +18°. The measurement results indicate that a wide scanning range from −73° to +18° is obtained, which is wider than the simulated results due to the fabrication and test errors. The *x*-directed vertical LP radiation performances in the *xoz*-plane for Port 2 are not shown here for brevity. Its simulated beam scans from +67° to −18°, while the measured result is from +70° to −18°.

Fig. 22 shows the simulated and measured radiation patterns for Port 3 at four operating states, i.e., RHCP, dual-polarization equal-amplitude dual-beam, dual-polarization unequal-amplitude dual-beam, single-polarization single-beam radiation. As seen, the measured curves are consistent with the simulated ones with a small frequency shift. For the first case in Fig. 22(c), an RHCP beam is realized in two orthogonal planes. Fig. 23(a) shows the simulated and measured axial ratio (AR) of the antenna for Port 3, which are less than 3 dB within the band of 27.6–28.9 GHz. Moreover, when the proposed coupler is an equal power divider, the second state of dual-polarization equal-amplitude dual-beam radiation is achieved, as illustrated in Fig. 22(a), (b) and (d). It can be observed that the antenna has a scanning coverage of 38° in each of the orthogonal planes. For example, in *xoz*-plane, the antenna scans from −35° to −2° for the backward quadrant, and 3° to 8° for the forward quadrant. For the third case, an unequal-amplitude dual-beam radiation is implemented when the coupler is an unequal power divider, as shown in Fig. 22(e). For the final case, a single-polarization single-beam radiation in the *xoz*-plane is achieved when the coupler is converted into a crossover, as shown in Fig. 22(f). For clearer demonstration, the simulated and measured amplitude imbalances of two beams of the proposed antenna exited by

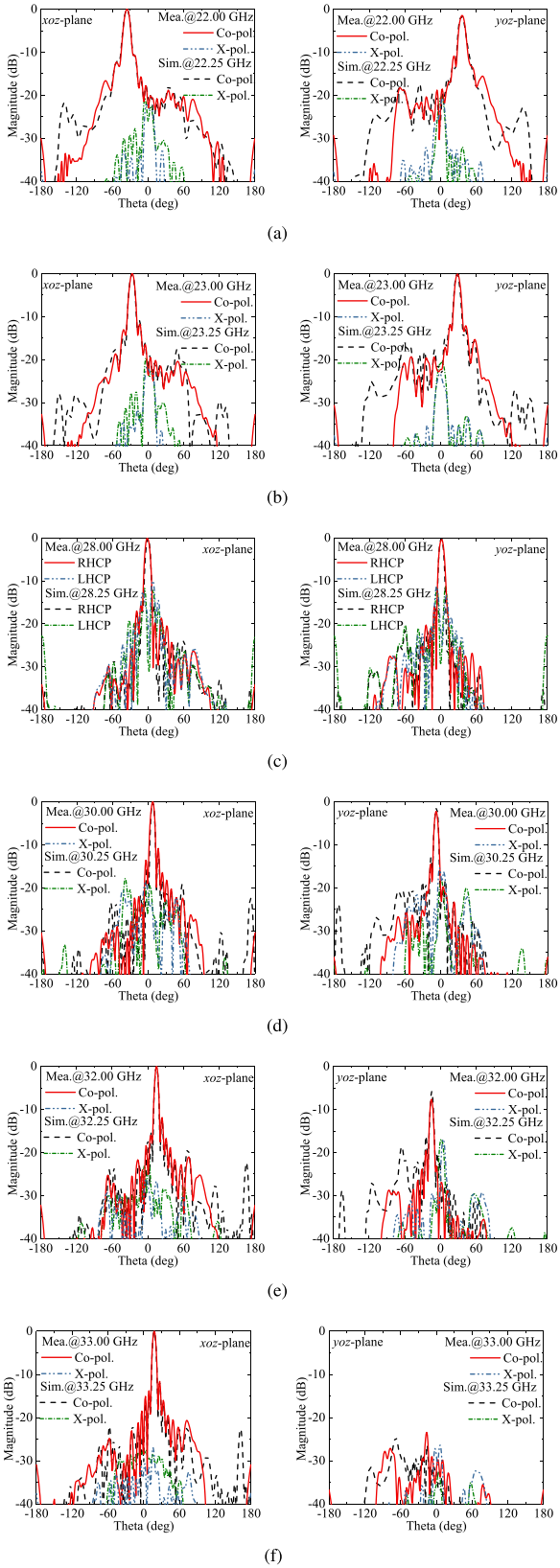

Fig. 22. Measured and simulated radiation patterns of the proposed 2-D LWA antenna excited by Port 3 at six different frequencies. (a) 22 GHz. (b) 23 GHz. (c) 28 GHz. (d) 30 GHz. (e) 32 GHz. (f) 33 GHz.

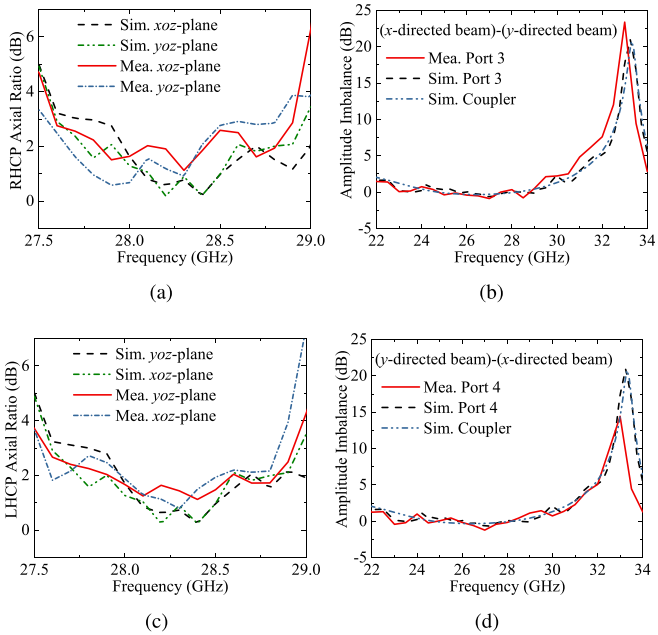

Fig. 23. (a) Simulated and measured RHCP axial ratio of the proposed antenna. (b) Simulated and measured amplitude imbalances of two beams of the proposed antenna excited by Port 3. (c) Simulated and measured LHCP AR of the proposed antenna. (d) Simulated and measured amplitude imbalances of two beams of the proposed antenna excited by Port 4.

Port 3 is shown in Fig. 23(b). As shown, the simulated and measured amplitude difference of the two beams of the antenna is consistent with the simulated amplitude difference between two output ports of the coupler. It is evident that the proposed coupler realized multiple functions, such as equal/unequal-amplitude coupler and crossover. The radiation patterns of the proposed antenna excited by Port 4 are not illustrated herein for brevity as it is similar to the case of Port 3. The AR performances and amplitude imbalances of the proposed antenna excited by Port 4 are illustrated in Fig. 23(c) and (d), respectively. It can be seen from Fig. 23 that the simulation results are basically consistent with the measured results.

Regarding the polarization discrimination, Figs. 21 and 22 show that the proposed antenna maintains a low cross-polarization level (<-20 dB) when the antenna operates in different polarization states, which indicates that the proposed antenna has a good polarization discrimination capability. This is due to the orthogonal arrangement of the proposed radiation aperture and the design of the feeding network. The orthogonal radiation aperture structure can reduce the interference between different polarization modes and improve the channel isolation [24]. Besides, the proposed feeding network is used to precisely control the excitation and propagation direction of EM waves. Furthermore, the seamless integration of the radiation aperture with the feeding network reduces unnecessary coupling and leakage, which further benefits the antenna to achieve a low cross-polarization characteristic.

In terms of the beam-scanning characteristics, the scanning angles of the proposed antenna excited by different input ports are shown in Fig. 24. As depicted in Fig. 24, there are versatile scanning angles for different ports. Nevertheless, a wide beam

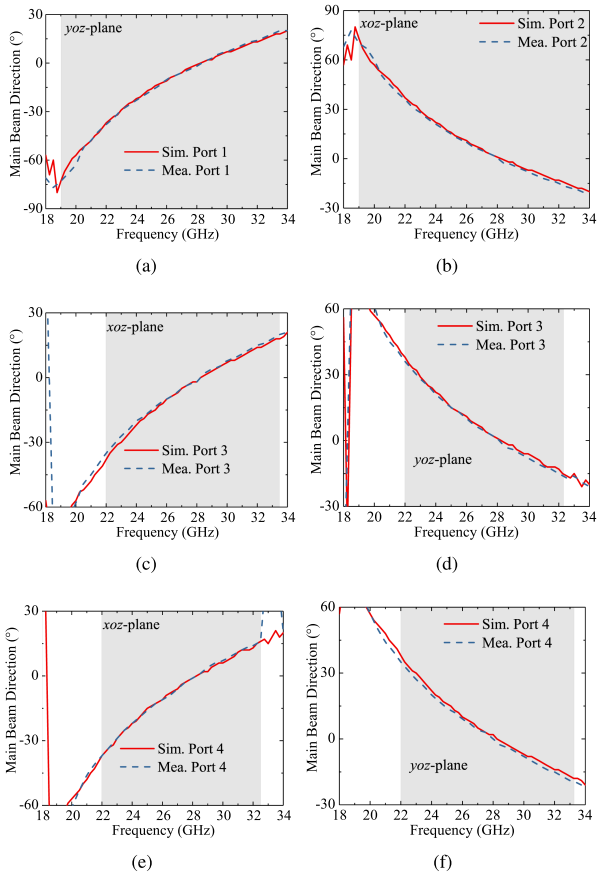

Fig. 24. Simulated and measured radiation angle for the proposed antenna excited by different input ports. (a) Port 1 at *yoz*-plane. (b) Port 2 at *xoz*-plane. (c) Port 3 at *xoz*-plane. (d) Port 3 at *yoz*-plane. (e) Port 4 at *xoz*-plane. (f) Port 4 at *yoz*-plane. (The gray region represents the operating frequency band of the proposed antenna).

scanning coverage through broadside direction (105° in *xoz*-plane & 108° in *yoz*-plane) is realized in this work. For detailed demonstration, the measured results are listed in Table I, including bandwidth, peak gain, coupler function, polarization states, number of beams, and scanning coverage. Table I shows that the proposed antenna features broad bandwidth (19–34 GHz), high antenna gain (23.6 dBi), versatile polarization and beam reconfigurability.

Table II presents a comparison of the proposed antenna with other reported reconfigurable antennas in order to illustrate the merits of the proposed antenna. As shown in Table II, the proposed antenna demonstrates much wider bandwidth (56.6%) than other reported LWA antennas. Compared with other reported PPW LWAs [20], [21], [22], [24], the proposed antenna has smaller radiation aperture size, but still keeps high gain (23.6 dBi). Although the antennas presented in [21] and [22] have higher gain, their aperture sizes are around 3.5 times larger than that of the proposed antenna. Table II shows that the proposed antenna has broadband and high-gain performance. This is mainly due to the complete suppression of OSB, the design of symmetrical array, the implementation of broadband low loss feeding network, and the seamless integration of the feeding network and the radiation aperture. In terms of the polarization states, the proposed antenna has seven available states. It can be seen from Table II that most of the reported PPW LWAs [20], [21], [22], [24] were designed to be single/dual-polarization antennas with a single fixed broadside beam. As for the SIW LWAs, the designs in [27] and [28] have six polarization states. However, their multi-polarized states are achieved by changing different extended couplers, which would increase the transmission loss and the measured complexity. Moreover, the amplitude difference of the proposed dual-polarization dual-beam antenna could be easily adjusted by controlling the power ratio between two output ports of the multifunction coupler. As for the scanning range, the proposed PPW LWA has a wide beam-scanning coverage through broadside direction (105° at *xoz*-plane & 108° at *yoz*-plane), while other reported PPW LWAs in [20], [22] and [24] do not have beam-scanning ability. From Table II, the scanning ranges of the LWAs in [26], [27], [28] are limited within the backward or forward regions due to the existence of OSB. In summary, due to the merits of broad bandwidth, high gain, polarization and radiation beam reconfigurability, wide beam coverage, and ease of fabrication, the proposed LWA is suitable for mmWave vehicular communication system.

The novelty of the proposed antenna over the work in [22] lies in the following aspects. In [22], two symmetrical slots are used to suppress the OSB, while two nonidentical slots are utilized to fully suppress the OSB in this work. The radiation aperture of the proposed antenna is also different from that of [22]. Two sub-arrays are arranged symmetrically by the middle line of the array to achieve the proposed 1-D array, while the uniform array arrangement is utilized in [22]. In addition, a single-layer offset parabolic reflector system is proposed in this work, while a two-layer feeding network is utilized in [22]. As for the polarization states, the proposed antenna has seven polarization states, while the reported antenna in [22] is a dual-polarization antenna. Besides, the proposed antenna has radiation beam reconfigurability, while the antenna in [22] does not have radiation beam reconfigurability. Furthermore, the bandwidth of the presented antenna in [22] is 1%. For the proposed antenna, a larger impedance bandwidth (56.6%) is obtained. Finally, the scanning range of the proposed antenna is much wider than that of the antenna in [22].

V. Conclusion

A broadband high-gain integrated antenna with polarization and radiation beam reconfigurability has been presented in this article. A shared-aperture 2-D LWA is designed for the realization of antenna polarization and beam reconfigurability. Depending upon its feeding scheme, the proposed antenna has the ability to change its polarization and radiation beam states. An antenna prototype has been designed, fabricated, and installed into an antenna measurement system for characterization. The measured results have a good match with the simulated ones, which verify the proposed design concept. Specifically, the proposed antenna supports linear-polarization single-beam (*y*-directed horizontal LP and *x*-directed vertical LP beam), circular-polarization single-beam (RHCP and LHCP beam), and dual-polarization

TABLE I
MEASURED RESULTS OF THE PROPOSED ANTENNA

Excited Port	Bandwidth	Peak Gain	Coupler Function	Polarization States	Number of Beams	Beam Scanning Range (Radiation Plane)
Port 1	19-34 GHz	23.6 dBi	Ineffective	*y*-Directed Horizontal LP	Single	Backward to Forward Through Broadside (-73° to +20° @ *yoz*-plane)
Port 2	19-34 GHz	23.3 dBi	Ineffective	*x*-Directed Vertical LP	Single	Backward to Forward Through Broadside (+70° to -21° @ *xoz*-Plane)
Port 3	27.6-28.9 GHz	20.4 dBic	Equal-Amplitude 90° Coupler	RHCP	Single	Broadside (-2° to 0° @ *xoz*-Plane & 2° to -2° @ *yoz*-Plane)
Port 3	22-27.6 GHz & 28.9-30.6 GHz	21.9 dBi	Equal-Amplitude Coupler	*x*-Directed Vertical LP & *y*-Directed Horizontal LP	Dual	Backward & Forward (-35° to -2° & +3° to +8° @ *xoz*-Plane & +36° to +2° & -2° to -8° @ *yoz*-Plane)
Port 3	30.6-32.25 GHz	21.4 dBi	Unequal-Amplitude Coupler	*x*-Directed Vertical LP & *y*-Directed Horizontal LP	Dual	Forward (+8° to +14° @ *xoz*-Plane & -8° to -15° @ *yoz*-Plane)
Port 3	32.25-33.5 GHz	22.5 dBi	Crossover	*x*-Directed Vertical LP	Single	Forward (+14° to +18° @ *xoz*-Plane)
Port 4	27.6-28.9 GHz	20 dBic	Equal-Amplitude 90° Coupler	LHCP	Single	Broadside (+2° to -2° @ *yoz*-Plane & -2° to 0° @ *xoz*-Plane)
Port 4	22-27.6 GHz & 28.9-31.2 GHz	21.3 dBi	Equal-Amplitude Coupler	*y*-Directed Horizontal LP & *x*-Directed Vertical LP	Dual	Backward & Forward (+35° to +2° & -3° to -13° @ *yoz*-Plane & -37° to -2° & +3° to +12° @ *xoz*-Plane)
Port 4	31.2-32.5 GHz	21.8 dBi	Unequal-Amplitude Coupler	*y*-Directed Horizontal LP & *x*-Directed Vertical LP	Dual	Forward (-13° to -16° @ *yoz*-Plane & +12° to +16° @ *xoz*-Plane)
Port 4	32.5-33.25 GHz	20.3 dBi	Crossover	*y*-Directed Horizontal LP	Single	Forward (-16° to -19° @ *yoz*-Plane)

TABLE II
COMPARISON BETWEEN THE PROPOSED ANTENNA AND OTHER REPORTED ANTENNAS

Ref.	Bandwidth (%)	Max. Gain (dBi/dBic)	Polarization Reconfigurability (Polarization States)	Number of Beams	Scanning Range	Peak Aperture Efficiency (%)	Radiation Aperture Volume (λ_0^3)
[20]	3.6	23	No (1)	Single	Broadside	N. A.	$7.2 \times 5.8 \times 0.14$
[21]	3.42 & 14.5	27.1 & 25.3	Yes (2)	Single	Broadside & 32° (-25° to -57°)	39.54% & 19.74%	$11 \times 9.4 \times 0.42$&$12 \times 10.3 \times 0.46$
[22]	1	26	Yes (2)	Single	Broadside	N. A.	$10.3 \times 10.3 \times 0.32$
[24]	6.6	24	Yes (2)	Single	Broadside	N. A.	$7 \times 7 \times 0.29$
[25]	N. A. (25.8 GHz)	22	Yes (2)	Single	Broadside	N. A.	$11.2 \times 5.2 \times 0.14$
[26]	16.7	14.85 & 13.55	Yes (4)	Single	±45° LP: 27.2° (30.3° to 3.1°) & CP: 26.1° (-29.2° to -3.1°)	N. A.	$8.7 \times 0.6 \times 0.06$
[27]	±45° LP: 36.9 & X/Y-Pol.: 41.4 & Dual-CP: 28.6	12	Yes (6)	Single	N. A.	N. A.	$3 \times 0.8 \times 0.03$
[28]	8.92	12.6	Yes (6)	Four	45° LP: 52° (20° to 72°) & X-Pol.: 62° (14° to 76°) & Y-Pol.: 60° (14° to 74°) & CP: 60° (16° to 76°)	N. A.	$6.8 \times 0.7 \times 0.06$
[29]	4	9 & 6	No (3)	Four	10° (-46° to -36°)	N. A.	$10.8 \times 0.1 \times 0.03$
This work	X/Y-Pol.: 56.6 & CP: 4.6 & Dual-LP: 22.6 & 14.7	23.6	Yes (7)	Single/Dual (Variable Amplitude)	X-Pol.: 91° (70° to -21°) & Y-Pol.: 93° (-73° to 20°) & CP: 4° (2° to -2°) & Dual-Pol.: 33° (-35° to -2°) & 11° (3° to 14°)	28.7%	$5.5 \times 5.5 \times 0.1$

* N.A.: Not available.
** λ_0 is the free-space wavelength at the lowest operating frequency.

dual-beam operation (equal/unequal-amplitude dual-LP radiation), showing the feasibility of realizing an integrated reconfigurable antenna. With its advantages of low cost, broad bandwidth, high gain, polarization, and radiation beam reconfigurability, the proposed antenna can potentially be employed for various mmWave vehicular communication application scenarios.

REFERENCES

[1] J. Wang et al., "Compact wideband circularly-polarized mechanically beam-steering antenna for Ka-band vehicular communications," *IEEE Trans. Veh. Technol.*, vol. 73, no. 3, pp. 3393–3403, Mar. 2024.

[2] J. Wang, C. Jiang, Z. Han, Y. Ren, and L. Hanzo, "Internet of Vehicles: Sensing-aided transportation information collection and diffusion," *IEEE Trans. Veh. Technol.*, vol. 67, no. 5, pp. 3813–3825, May 2018.

[3] L. Zhang et al., "A single-layer 10–30 GHz reflectarray antenna for the Internet of Vehicles," *IEEE Trans. Veh. Technol.*, vol. 71, no. 2, pp. 1480–1490, Feb. 2022.

[4] Z. Wang, S. Liu, and Y. Dong, "Compact wideband pattern reconfigurable antennas inspired by end-fire structure for 5G vehicular communication," *IEEE Trans. Veh. Technol.*, vol. 71, no. 5, pp. 4655–4664, May 2022.

[5] J. Yang, J. Li, S. Zhou, D. Li, and G. Yang, "A polarization and frequency reconfigurable microstrip antenna for vehicular communication system application," *IEEE Trans. Veh. Technol.*, vol. 72, no. 1, pp. 623–631, Jan. 2023.

[6] M. Nouri, H. Behroozi, A. Jafarieh, S. A. Aghdam, M. J. Piran, and N. K. Mallat, "A learning-based dipole Yagi-Uda antenna and phased array antenna for mmWave precoding and V2V communication in 5G systems," *IEEE Trans. Veh. Technol.*, vol. 72, no. 3, pp. 2789–2803, Mar. 2023.

[7] M. Marcus and B. Pattan, "Millimeter wave propagation: Spectrum management implications," *IEEE Microw. Mag.*, vol. 6, no. 2, pp. 54–62, Jun. 2005.

[8] Y. Zhang, J. -Y. Deng, D. Sun, J. -Y. Yin, and L. -X. Guo, "Compact slow-wave SIW H-plane horn antenna with increased gain for vehicular millimeter wave communication," *IEEE Trans. Veh. Technol.*, vol. 70, no. 7, pp. 7289–7293, Jul. 2021.

[9] Y. -X. Sun, "Large frequency ratio antennas based on dual-function periodic slotted patch and its quasi-complementary structure for vehicular 5G communications," *IEEE Trans. Veh. Technol.*, vol. 72, no. 7, pp. 8303–8312, Jul. 2023.

[10] D. Shin, W. -H. Lim, and H. L. Lee, "Highly integrated in-band full-duplex TRx antennas for mmWave V2X communications," *IEEE Trans. Veh. Technol.*, vol. 72, no. 5, pp. 6404–6411, May 2023.

[11] C. J. Ma, B. J. Xiang, S. Y. Zheng, and Y. M. Pan, "A miniaturized planar multibeam antenna for millimeter-wave vehicular communication," *IEEE Trans. Veh. Technol.*, vol. 72, no. 3, pp. 3611–3621, Mar. 2023.

[12] K. L. Chung et al., "Three-element circularly polarized MIMO antenna with self-decoupled probing method for B5G-V2X communications," *Alexandria Eng. J.*, vol. 70, pp. 553–567, May 2023.

[13] A. A. Oliner and D. R. Jackson, "Leaky-wave antennas," in *Antenna Engineering Handbook*, 4th ed., J. Volakis, Ed. New York, NY, USA: McGraw–Hill, 2007.

[14] Y. Cao, S. Yan, J. Li, and J. Chen, "A pillbox based dual circularly-polarized millimeter-wave multi-beam antenna for future vehicular radar applications," *IEEE Trans. Veh. Technol.*, vol. 71, no. 7, pp. 7095–7103, Jul. 2022.

[15] G. Zhang, Q. Zhang, Y. Chen, and R. D. Murch, "High-scanning-rate and wide-angle leaky-wave antennas based on glide-symmetry Goubau line," *IEEE Trans. Antennas Propag.*, vol. 68, no. 4, pp. 2531–2540, Apr. 2020.

[16] S. Ge, Q. Zhang, A. K. Rashid, Y. Zhang, H. Wang, and R. Murch, "A compact full-space scanning leaky-wave antenna with stable peak gain," *IEEE Trans. Antennas Propag.*, vol. 69, no. 10, pp. 6924–6929, Oct. 2021.

[17] X. Li et al., "Archimedean spiral slotted leaky-wave antenna," *IEEE Trans. Antennas Propag.*, vol. 70, no. 5, pp. 3208–3222, May 2022.

[18] T. Wang, L. Liu, H. Ni, L. Zhu, and G. Q. Luo, "A full-angle scanning leaky wave antenna based on odd-mode SSPP from backfire to endfire," *IEEE Trans. Antennas Propag.*, vol. 71, no. 11, pp. 8570–8579, Nov. 2023.

[19] K. Hashimoto, J. Hirokawa, and M. Ando, "A post-wall waveguide center-feed parallel plate slot array antenna in the millimeter-wave band," *IEEE Trans. Antennas Propag.*, vol. 58, no. 11, pp. 3532–3538, Nov. 2010.

[20] N. Bayat-Makou, K. Wu, and A. A. Kishk, "Single-layer substrate-integrated broadside leaky long-slot array antennas with embedded reflectors for 5G systems," *IEEE Trans. Antennas Propag.*, vol. 67, no. 12, pp. 7331–7339, Dec. 2019.

[21] Y. -W. Wu, Z. -W. Miao, G. Q. Luo, and Z.-C. Hao, "Planar millimeter-wave shared-aperture self-diplexing antenna with small frequency ratio and high isolation," *IEEE Trans. Antennas Propag.*, vol. 69, no. 12, pp. 8979–8984, Dec. 2021.

[22] Y. J. Cheng, J. Wang, and X. L. Liu, "94 GHz substrate integrated waveguide dual-circular-polarization shared-aperture parallel-plate long-slot array antenna with low sidelobe level," *IEEE Trans. Antennas Propag.*, vol. 65, no. 11, pp. 5855–5861, Nov. 2017.

[23] X. -L. Lu, H. Zhang, S. -M. Gu, H. Liu, X. -C. Wang, and W. -Z. Lu, "A dual-polarized cross-slot antenna array on a parallel-plate waveguide with compact structure and high efficiency," *IEEE Antennas Wireless Propag. Lett.*, vol. 17, no. 1, pp. 8–11, Jan. 2018.

[24] Q. -C. Ye, Y. -M. Zhang, J. -L. Li, G. F. Pedersen, and S. Zhang, "High-isolation dual-polarized leaky-wave antenna with fixed beam for full-duplex millimeter-wave applications," *IEEE Trans. Antennas Propag.*, vol. 69, no. 11, pp. 7202–7212, Nov. 2021.

[25] S. Park, Y. Okajima, J. Hirokawa, and M. Ando, "A slotted post-wall waveguide array with interdigital structure for 45° linear and dual polarization," *IEEE Trans. Antennas Propag.*, vol. 53, no. 9, pp. 2865–2871, Sep. 2005.

[26] Y. J. Cheng, W. Hong, and K. Wu, "Millimeter-wave half mode substrate integrated waveguide frequency scanning antenna with quadri-polarization," *IEEE Trans. Antennas Propag.*, vol. 58, no. 6, pp. 1848–1855, Jun. 2010.

[27] Y. Dong and T. Itoh, "Substrate integrated composite right-/left-handed leaky-wave structure for polarization-flexible antenna application," *IEEE Trans. Antennas Propag.*, vol. 60, no. 2, pp. 760–771, Feb. 2012.

[28] A. Sarkar, S. Mukherjee, A. Sharma, A. Biswas, and M. Jaleel Akhtar, "SIW-based quad-beam leaky-wave antenna with polarization diversity for four-quadrant scanning applications," *IEEE Trans. Antennas Propag.*, vol. 66, no. 8, pp. 3918–3925, Aug. 2018.

[29] M. Wang, H. C. Wang, S. C. Tian, H. F. Ma, and T. J. Cui, "Spatial multi-polarized leaky-wave antenna based on spoof surface plasmon polaritons," *IEEE Trans. Antennas Propag.*, vol. 68, no. 12, pp. 8168–8173, Dec. 2020.

[30] M. Ettorre, R. Sauleau, and L. Le Coq, "Multi-beam multi-layer leaky-wave SIW pillbox antenna for millimeter-wave applications," *IEEE Trans. Antennas Propag.*, vol. 59, no. 4, pp. 1093–1100, Apr. 2011.

[31] A. Al-Bassam, S. Otto, D. Heberling, and C. Caloz, "Broadside dual-channel orthogonal-polarization radiation using a double-asymmetric periodic leaky-wave antenna," *IEEE Trans. Antennas Propag.*, vol. 65, no. 6, pp. 2855–2864, Jun. 2017.

[32] J. Liu, W. Zhou, and Y. Long, "A simple technique for open-stopband suppression in periodic leaky-wave antennas using two nonidentical elements per unit cell," *IEEE Trans. Antennas Propag.*, vol. 66, no. 6, pp. 2741–2751, Jun. 2018.

[33] D. M. Pozar, *Microwave Engineering*, 4th ed. Hoboken, NJ, USA: Wiley, 2011.

Yaling Chen (Member, IEEE) is currently working toward the Ph.D. degree in information and communication engineering with Shenzhen University, Shenzhen, China. Her research interests include mmWave/THz antennas, leaky-wave antennas, and surface-wave antennas.

Long Zhang (Member, IEEE) received the B.S. and M.S. degrees in electrical engineering from the Huazhong University of Science and Technology (HUST), Wuhan, China, in 2009 and 2012, respectively, and the Ph.D. degree in electronic engineering from the University of Kent, Canterbury, U.K, in 2017. In 2018, he was a Research Fellow with Poly-Grames Research Center, Polytechnique Montreal, Montreal, QC, Canada. He is currently an Associate Professor with the College of Electronics and Information Engineering, Shenzhen University, Shenzhen, China. His research interests include millimeter-wave antennas and arrays, tightly coupled arrays, reflectarrays and transmitarrays, characteristic mode theory, and machine-learning methods for antenna and metasurface design. Dr. Zhang was a TPC Member and the Session Chair for several international conferences. He was also a Lead Guest Editor of *Electronics Letters* for a Special Issue on "Wideband/Multiband Millimeter-Wave Antennas for 5G/6G and Radar Applications" in 2023. He is also a Reviewer for several technique journals.

Yejun He (Senior Member, IEEE) received the Ph.D. degree in information and communication engineering from the Huazhong University of Science and Technology (HUST), Wuhan, China, in 2005. From 2005 to 2006, he was a Research Associate with the Department of Electronic and Information Engineering, The Hong Kong Polytechnic University, Hong Kong. From 2006 to 2007, he was a Research Associate with the Department of Electronic Engineering, Faculty of Engineering, The Chinese University of Hong Kong, Hong Kong. In 2012, he joined the Department of Electrical and Computer Engineering, University of Waterloo, Waterloo, ON, Canada, as a Visiting Professor. From 2013 to 2015, he was an Advanced Visiting Scholar (Visiting Professor) with the School of Electrical and Computer Engineering, Georgia Institute of Technology, Atlanta, GA, USA. From 2023 to 2024, he was an Advanced Research Scholar (Visiting Professor) with the Department of Electrical and Computer Engineering, National University of Singapore, Singapore.

Since 2006, Dr. He has been a Faculty with Shenzhen University, Shenzhen, China, where he is currently a Full Professor with the College of Electronics and Information Engineering. He is also the Director with Sino-British Antennas and Propagation Joint Laboratory, Ministry of Science and Technology (MOST), China, Guangdong Engineering Research Center of Base Station Antennas and Propagation, and also with the Shenzhen Key Laboratory of Antennas and Propagation, and the Chair of IEEE Antennas and Propagation Society-Shenzhen Chapter. He was also selected as a Leading Talent in the "Guangdong Special Support Program" and the Shenzhen "Pengcheng Scholar" Distinguished Professor, China, in 2024 and 2020, respectively. He has authored or coauthored more than 330 refereed journal and conference papers and seven books and holds over 20 patents. His research interests include wireless communications, antennas, and radio frequency. He is the Principal Investigator of more than 40 current or finished research projects, including the National Natural Science Foundation of China, the Science and Technology Program of Guangdong Province, and the Science and Technology Program of Shenzhen City. Dr. He was the recipient of the Shenzhen Overseas High-Caliber Personnel Level B (Peacock Plan Award B) and Shenzhen High-Level Professional Talent (Local Leading Talent), Second Prize of Guangdong Provincial Science and Technology Progress Award in 2023, 10th Guangdong Provincial Patent Excellence Award in 2023, Second Prize of Shenzhen Science and Technology Progress Award in 2017, and the Three Prize of Guangdong Provincial Science and Technology Progress Award in 2018, and 2022 IEEE APS Outstanding Chapter Award.

Dr. He is also an Associate Editor for IEEE TRANSACTIONS ON ANTENNAS AND PROPAGATION, IEEE TRANSACTIONS ON VEHICULAR TECHNOLOGY, IEEE TRANSACTIONS ON MOBILE COMPUTING, *IEEE Antennas and Propagation Magazine*, IEEE ANTENNAS AND WIRELESS PROPAGATION LETTERS, *International Journal of Communication Systems*, *China Communications*, and *ZTE Communications*. He was a Reviewer for various journals, such as IEEE TRANSACTIONS ON VEHICULAR TECHNOLOGY, IEEE TRANSACTIONS ON COMMUNICATIONS, IEEE TRANSACTIONS ON INDUSTRIAL ELECTRONICS, IEEE TRANSACTIONS ON ANTENNAS AND PROPAGATION, IEEE WIRELESS COMMUNICATIONS, IEEE COMMUNICATIONS LETTERS, *International Journal of Communication Systems*, and *Wireless Personal Communications*. He was a Technical Program Committee Member or a Session Chair for various conferences, including the IEEE Global Telecommunications Conference (GLOBECOM), IEEE International Conference on Communications (ICC), IEEE Wireless Communication Networking Conference (WCNC), and IEEE Vehicular Technology Conference (VTC). He was the TPC Chair for IEEE ComComAp 2021, and General Chair for IEEE ComComAp 2019. He was selected as a Board Member of the IEEE Wireless and Optical Communications Conference (WOCC). He was the TPC Co-Chair for WOCC 2023/2022/2019/2015, APCAP 2023, UCMMT 2023, ACES-China2023, and NEMO 2020. He was the Executive Chair of 2024 IEEE International Workshop of Radio Frequency and Antenna Technologies (RFAT 2024). He is also the Executive Chair of 2025 IEEE International Workshop of Radio Frequency and Antenna Technologies (RFAT 2025). He acted as the Publicity Chair of several international conferences such as the IEEE PIMRC 2012 and IEEE MAPE 2024. He is also Fellow of the China Institute of Communications, and Fellow of IET.

Zhi Ning Chen (Fellow, IEEE) received the B.Eng., M.Eng., and Ph.D. degrees in electrical engineering from the Institute of Communications Engineering (ICE), China, in 1985, 1988, and 1993, respectively, and the second Ph.D. degree from the University of Tsukuba, Tsukuba, Japan, in 2003. He is currently a Provost's Chair Professor with the Department of Electrical and Computer Engineering and the Founder and Director with Advanced Research and Technology Innovation Center, National University of Singapore, Singapore. Besides the concurrent Guest Professorships with aboard universities, he has also provided twelve local and overseas companies with technical consultancy service as Technical Advisor, Guest Professor, and Chief Scientist. In 2005, he was the Founding General Chairs of International Workshop on Antenna Technology (iWAT), International Symposium on InfoComm & Mechatronics Technology in Bio-Medical & Healthcare Application (IS 3T-in-3 A) in 2010, International Microwave Forum (IMWF) in 2010, Asia-Pacific Conference on Antennas and Propagation (APCAP) in 2012, and Marina Forum (Mar-For) in 2021. He has authored or coauthored more than 710 academic papers and six books. He is holding 35 granted and filed patents and has completed more than 43 technology licensed deals with industry. His research interests include the translational research of electromagnetic metamaterials and the applications of algorithms, in particular, prior-knowledge-guided deep learning-enabled optimization and generative methods to antenna design. He is pioneering in developing small and wideband and ultra-wideband antennas, wearable and implanted medical antennas, package antennas, near-field antennas and coils, three-dimensional integrated LTCC arrays, microwave lens antennas, microwave metamaterial-metasurface antennas for communications, sensing, and imaging systems. Dr. Chen was the recipient of the IEEE Antennas and Propagation Society (APS) John Kraus Antenna Award in 2021. Since 2016, he has been a Distinguished Lecturer with IEEE Council on RFID and was the founding Vice President during 2015–2020. He was an Associate Editor for IEEE TRANSACTION ON ANTENNAS AND PROPAGATION, was also as a Distinguished Lecturer with IEEE APS, and the Members of Fellow Committee and New Direction Committee. In 2008, he was a Chair of IEEE Singapore MTT/AP Chapter and the Chair of IEEE Singapore RFID Chapter in 2017. He is also a Member of IEEE APS AdCom and IEEE Future Networks Initiative Technology Focus Editorial Board. In 2019, he was elevated to the Fellow of the Academy of Engineering, Singapore, Fellow of the IEEE for his contribution to small and broadband antennas for wireless applications in 2007, and Fellow and Vice President of Asia-Pacific Artificial Intelligence Association.